

Friction models incorporating thermal effects in highly precision actuators

J. W. Li,^{1,2,3} X. B. Chen,^{2,3} Q. An,¹ S. D. Tu,¹ and W. J. Zhang^{1,2,3,a)}

¹*School of Mechanical and Power Engineering, East China University of Science and Technology, Shanghai 200237, People's Republic of China*

²*Department of Mechanical Engineering, University of Saskatchewan, Saskatoon, Saskatchewan S7N5A9, Canada*

³*Division of Biomedical Engineering, University of Saskatchewan, Saskatoon, Saskatchewan S7N5A9, Canada*

(Received 3 December 2008; accepted 15 March 2009; published online 14 April 2009)

This paper presents two models based on the LuGre model for friction with consideration of thermal effects. In Model I, parameters in the LuGre model are considered as temperature dependent. In Model II, parameters in the LuGre model are considered as temperature independent; while a temperature-dependent function is added to the temperature-independent LuGre model. Both models are experimentally evaluated, which shows that both can effectively incorporate thermal effects but Model II has better accuracy. Since these models are developed in the context of the motion system, they should be readily incorporated in motion control algorithms for effective control of motion systems with friction if temperature rise is significant in these systems. © 2009 American Institute of Physics. [DOI: 10.1063/1.3115208]

I. INTRODUCTION

Friction modeling is important in control of motion systems that require high accuracy and precision. In industry, the negative effect of friction is usually minimized by reducing the friction coefficient, such as improving quality of contact surfaces, using lubricants, and optimizing structure design. However, for some friction-driven systems (e.g., stick slip actuators), friction force should not be reduced because it provides a driving force for these systems to work.^{1,2} Both unwanted and wanted frictions need to be understood and predicted through modeling. It is known that friction force is a function of velocity, load, displacement, temperature of two contact surfaces, and the surface properties, many of which are time dependent and/or temperature dependent.³⁻⁸ Therefore, accurate modeling of friction is very difficult. In the current literature, the models such as Dahl model,⁹ LuGre model,¹⁰ Elastoplastic friction model,¹¹ Leuven model,^{12,13} and Generalized Maxwell-Slip model^{14,15} are available to represent complex friction phenomena; however they have not considered thermal effects on friction (i.e., how temperature rises affect friction).

Regarding the temperature-dependency property of friction, Sang *et al.*⁸ studied the dependency of friction on temperature for single or a couple of asperities using an atomic force microscope. They experimentally found that the friction force decreases (from 0.46 to 0.18 nN) with the increase in temperature (from 53 to 373 K). Their study has further shown that friction force is a function of velocity and temperature, especially $F_r \propto \text{const} - T^{2/3} |\ln(v/T)|^{2/3}$, where F_r is friction force, *const* is a constant, v is relative velocity, and T is temperature. Their finding may only be valid for a single

asperity situation. Cristol-Bulthé *et al.*⁴ experimentally studied the variation in friction due to thermal effects in a stop-braking system. Their study has shown that friction coefficient increases from 0.26 to 0.3 when the temperature increases and decreases from 0.3 to 0.29 when the temperature decreases. They have, however, not developed a friction model to incorporate such thermal effects. Childs³ developed a friction model for metal cutting. His study has shown that the friction force in his system is dependent on the cutting speed and temperature. Temperature has, however, not been considered in his friction model.

The present study aimed to develop the friction model that can incorporate thermal effects in the context of high precision actuator systems. The study was based on the LuGre model because it has fewer parameters yet excellent accuracy in modeling of friction behaviors.^{2,10} Two friction models, which incorporate thermal effects in the context of the stick-slip motion system, were thus developed called Model I and Model II, respectively. Particularly, in Model I, the parameters of the LuGre model were considered to be temperature dependent and subsequently, the relationships between these parameters and temperature were obtained using the system identification techniques. Model II has two parts: one part is the temperature-independent LuGre model, while the other part is a temperature-dependent component, which has two linear segments and is further determined using the system identification techniques.

To assist in the development of these two models as well as to verify them, the piezoelectric stick-slip actuator (PE-SSA) system developed in our previous work⁶ was taken as a test bed. In the remainder of this paper, the next section outlines the PE-SSA system as well as its dynamic model, followed by a detailed description of model development, experimental validation and finally, a conclusion.

^{a)} Author to whom correspondence should be addressed. Electronic mail: chris.zhang@usask.ca.

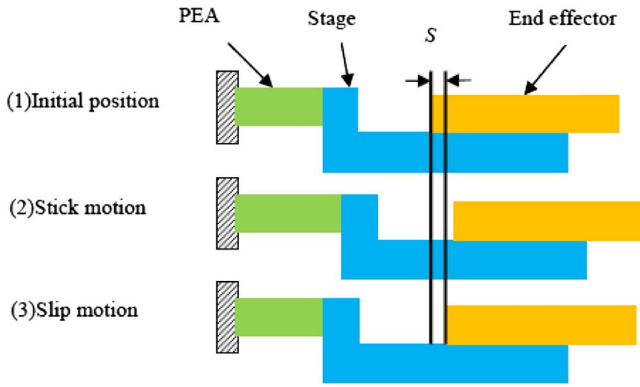


FIG. 1. (Color online) The working process of the PE-SSA.

II. THE PE-SSA SYSTEM AND ITS DYNAMIC MODEL

The PE-SSA is the hybridization of the piezoelectric actuator (PEA) and the stick slip actuator (SSA). It has the advantages of both high resolution (several nanometers) contributed by the PEA and long range (several centimeters) contributed by the SSA.^{1,6} The operation of the PE-SSA is demonstrated in Fig. 1. At position (1), a potential is applied to the PEA, and this leads to a (relatively slow) expansion of the PEA, which further pushes the stage moving to position (2) due to the static friction between the stage and the end effector. The motion in this period is called “stick” motion. When the voltage is released quickly, the PEA contracts quickly, and a sliding between the end effector and stage takes place due to the inertia of the end effector. The motion in this period is called “slip” motion. As the result of the stick and slip motion, the end effector has a “net” displacement denoted by S (see Fig. 1). If the aforementioned process is repeated periodically, the end effector will generate a series of motion to the right (S_1, S_2, \dots, S_n ; n is the number of cycles) as long as the physical structure allows. In the following, we outline a dynamic model of the PE-SSA system.

Adriaens *et al.*¹⁶ showed that the PEA and stage can be modeled as a spring-mass-damper system, which was validated in our previous study.² The governing equations of this spring-mass-damper system are given in Eq. (1) as follows:

$$m\ddot{x}_p + c\dot{x}_p + kx_p = T_{em}u_p \quad (1)$$

with

$$\begin{cases} m = \frac{4m_p}{\pi^2} + m_s \\ c = c_p + c_s \\ k = k_p + k_s \end{cases}, \quad (2)$$

where m is equivalent mass, c is the equivalent damping coefficient, k is the equivalent stiffness, m_p is the mass of PEA, c_p is the damping coefficient of PEA, k_p is the stiffness of PEA, m_s is the mass of stage, c_s is the damping coefficient of the stage, k_s is the stiffness of stage, x_p is the displacement of the PEA, T_{em} is the electromechanical transducer ratio, and u_p is the applied voltage on the PEA.¹⁶ More details on this model can be found in Ref. 16. Equation (1) can be further written as

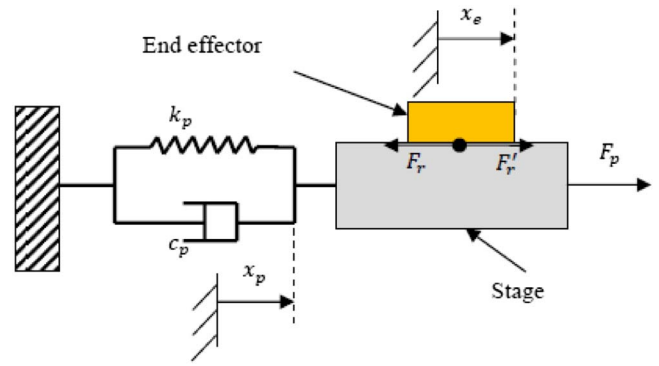


FIG. 2. (Color online) Physical model of the PE-SSA system.

$$\ddot{x}_p + 2\xi\omega_n\dot{x}_p + \omega_n^2x_p = K\omega_n^2u_p \quad (3)$$

with

$$\begin{cases} \frac{c}{m} = 2\xi\omega_n \\ \frac{k}{m} = \omega_n^2 \\ \frac{T_{em}}{m} = K\omega_n^2 \end{cases}, \quad (4)$$

where ξ is the damping ratio, ω_n is the natural frequency, and K is the amplification coefficient. The parameters in Eq. (4) were obtained from the step responses of the system: $\xi = 0.2488$, $\omega_n = 6685.5$ rad/s, and $K = 0.096 \times 10^{-6}$ m/V.

In the PE-SSA (i.e., the PE system together with the stage and end effector; see Fig. 2), the friction force F_r between the end effector and stage is applied on the stage. Then, we can get the model of the PE-SSA by extending Eq. (1), i.e.,

$$m\ddot{x}_p + c\dot{x}_p + kx_p + F_r = F_p. \quad (5)$$

The friction force on the end effector (F'_r) is given by

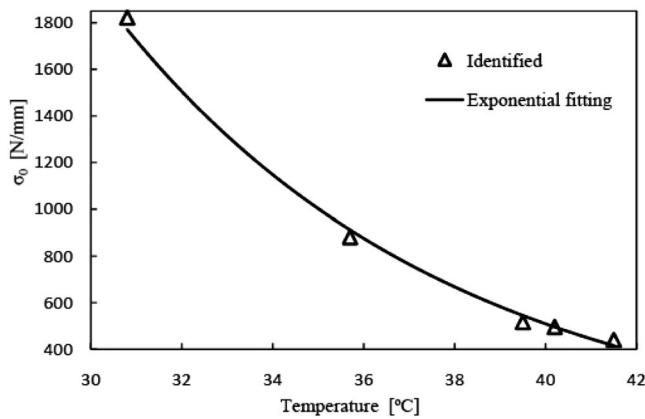
$$\begin{cases} F'_r = m_e\ddot{x}_e \\ F'_r = -F_r \\ x_e = x_p + x_{pe} \end{cases}, \quad (6)$$

where x_e is the displacement of the end effector, and x_{pe} the relative displacement between the end effector and stage. In this study, the stick-slip induced friction force F'_r was further modeled using the LuGre model (F_r^L : the LuGre friction); see Eq. (7). In the LuGre model, it is assumed that the two contact surfaces consist of many asperities that can be modeled as “bristles.” The friction force is thus related to the properties of these bristles and is expressed as follows:^{10,11}

$$F'_r = F_r^L \quad (7)$$

$$\begin{cases} F_r^L = \sigma_0 z + \sigma_1 \dot{z} + \sigma_2 \dot{x}_{pe} \\ \dot{z} = \dot{x}_{pe} \left(1 - \frac{\sigma_0}{|f_c|} \text{sgn}(\dot{x}_{pe}) \times z \right) \end{cases}, \quad (8)$$

where σ_0 is the stiffness of the bristles, z is the average bristle deflection, σ_1 is the damping coefficient of the bristle, σ_2 is the contact damping coefficient, and f_c is the Coulomb

FIG. 3. σ_0 vs temperature.

friction. In this study, σ_2 is regarded as 0 because \dot{x}_{pe} is very small.²

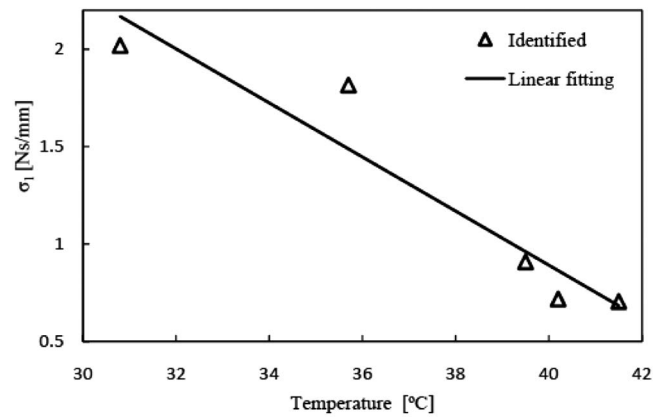
III. MODELING OF THERMAL EFFECTS

Studies have shown that the friction force, which is associated with the interaction between two contact surfaces, is temperature dependent.^{3,4,8} Two methods to incorporate thermal effects on friction were thus developed and are discussed in this section.

A. Model I

According to the LuGre model, the parameters σ_0 , σ_1 , and f_c represent the mechanical properties of materials. In this study, the materials of two contact objects, i.e., friction plates and end effector, are Cu–Cu. Studies have shown that the properties (e.g., resonance frequency, hardness, and Young's modulus) of metal materials vary with the change in temperature.^{17–19} Thus, the parameters σ_0 , σ_1 , and f_c in the LuGre model were considered as functions of temperature, i.e., $\sigma_0 = \varphi_0(T)$, $\sigma_1 = \varphi_1(T)$, and $f_c = \varphi_c(T)$. In this study, the parameters σ_0 , σ_1 , and f_c were determined in MATLAB by using the parameter estimation method similar to the one reported in our previous work.^{2,17} Briefly, a Simulink model was developed based on Eqs. (1)–(8) and a *M*-file program employing the function of nonlinear fit in MATLAB was developed to estimate the parameters σ_0 , σ_1 , and f_c based on nonlinear least-squares regression. The Simulink model was to predict the displacement of the PE-SSA for given input by using the parameter values inputted from the *M*-file program; while the *M*-file program was to estimate the parameters by starting with an initial guess and then altering the guess until the difference between the measured displacements and the model predictions is less than a predefined value. The parameters of the model were estimated for different temperatures and the variations of these parameters with respect to temperature are plotted in Figs. 3–5.

Studies have further shown that the variations in mechanical properties of metal materials with respect to temperature could be approximated with exponential or linear fitting. For instance, the tensile strength and yield strength of the lead-tin alloy decrease with the increase in temperature;¹⁸ the relationship between tensile strength and temperature ap-

FIG. 4. σ_1 vs temperature.

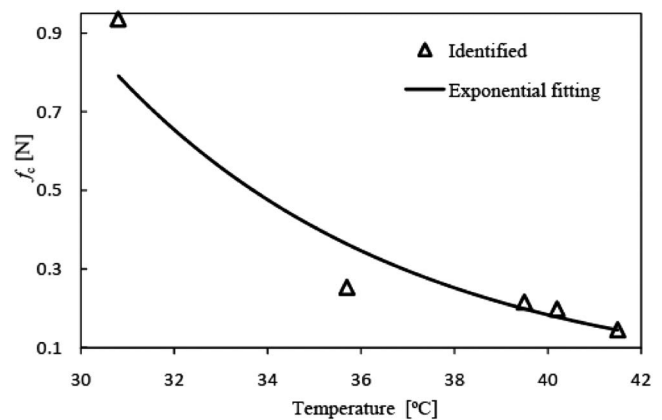
pears quite exponential and the variation in yield strength with temperature appears quite linear. Lebedev *et al.*¹⁹ experimentally observed that Young's modulus of copper linearly decreases with the increase in temperature. Fang *et al.*²⁰ studied the effects of temperature on the atomic-scale nanoindentation process using a three-dimensional molecular dynamics model. Their results showed that Young's modulus and hardness of copper linearly decrease with the increase in temperature. Therefore, in our case, $\sigma_0 = \varphi_0(T)$, $\sigma_1 = \varphi_1(T)$, and $f_c = \varphi_c(T)$ are thus likely to be described using either an exponential equation or a linear equation. In this study, the following equations were found by us to best approximate the relationships of the three parameters σ_0 , σ_1 , and f_c with respect to temperature, and they are given below,

$$\varphi_0(T) = 115072e^{-0.136T} \quad (9)$$

$$\varphi_1(T) = -0.138T + 6.445 \quad (10)$$

$$\varphi_c(T) = 106.04e^{-0.159T}. \quad (11)$$

One potential problem with the above approach is that in the LuGre model, these parameters are not equally sensitive to temperature,¹⁰ while the approach above in fact treats them as their being equally sensitive to temperature. The accuracy with this method may also be compromised due to the complexity of computation in parameters identification which involves multiscale parameters and solving a mixed differential and algebraic equation.

FIG. 5. f_c vs temperature.

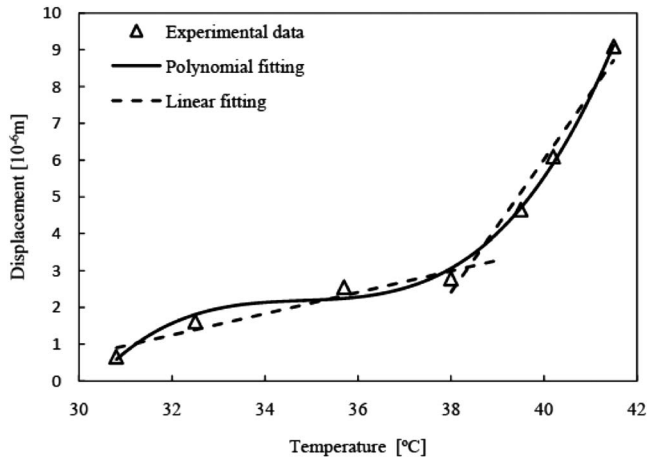


FIG. 6. Relationship between displacement and temperature.

B. Model II

We considered that the temperature-dependent parameters in the LuGre model may be somewhat expressed by Taylor series; as such the friction force owing to temperature change and those other factors (e.g., velocity, etc.) can be represented with two parts: friction force without temperature change and friction force with temperature change, i.e.,

$$F_r' = F_r^L + \Delta F_r^T, \tag{12}$$

where F_r^L is the friction force based on the temperature-independent LuGre model (i.e., the parameters in the LuGre model are regarded as independent of temperature) and ΔF_r^T is temperature dependent or called the thermal-induced friction force, i.e., $\Delta F_r^T = f(T)$. Further, ΔF_r^T was obtained by the following steps. First, the displacements of the PE-SSA were measured at different temperatures, and as a result, Fig. 6 was plotted. From this figure, it can be seen that either two linear relations or a polynomial could well represent the relationship between the displacement and temperature (in our study, two linear relations were employed). Second, from Eqs. (1)–(8) and (12), we can obtain the relationship between ΔF_r^T and the displacement, as plotted in Fig. 7. This relationship is quite linear especially when the change in friction force is within the range of (0–0.5 N), which covers the

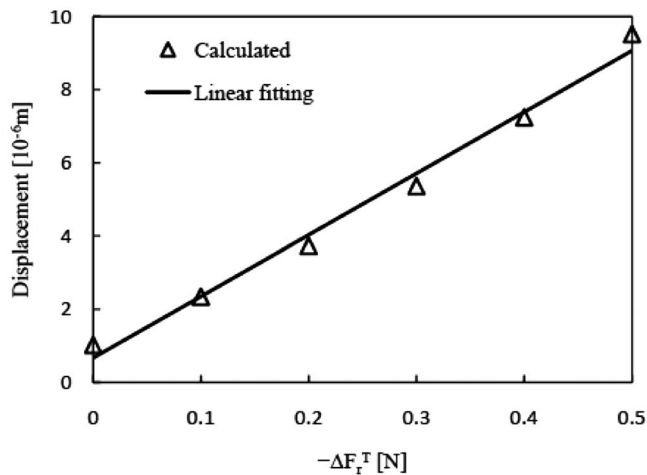


FIG. 7. Relationship between displacement and thermal-induced friction.

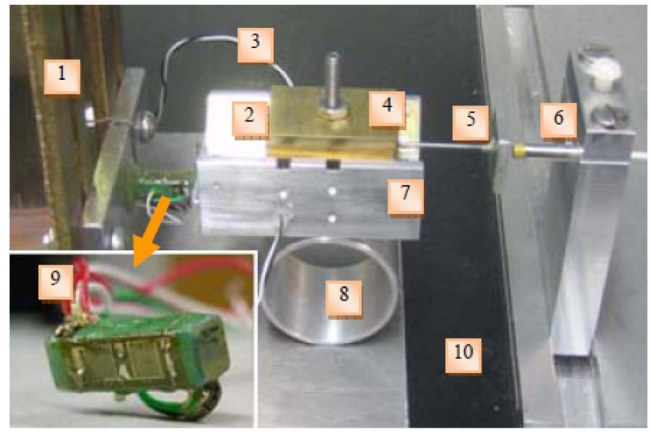


FIG. 8. (Color online) Experimental system of the PE-SSA (Ref. 6) (1: frames; 2: friction plates; 3: temperature sensor; 4: weights; 5: end effector; 6: displacement sensor; 7: stage; 8: wheel; 9: PEA; 10: vibration isolation test bed).

primary displacement range of our test system, and thus this relationship can be readily approximated by a linear equation. Third, by combining Figs. 6 and 7, we can obtain the relationship between the temperature and thermal-induced friction (ΔF_r^T),

$$\Delta F_r^T = \begin{cases} \frac{-0.29T + 8.704}{16.8} & (30.0 \leq T \leq 38.4 \text{ } ^\circ\text{C}) \\ \frac{-1.8T + 66.678}{16.8} & (38.4 < T \leq 41.5 \text{ } ^\circ\text{C}) \end{cases} . \tag{13}$$

IV. MODEL VALIDATION AND DISCUSSION

The PE-SSA prototype described in our previous study⁶ was employed for model validation. The displacements of the actuator were measured with a KAMAN instrument, which is based on the eddy-current inductive principle and has the submicron resolution. The measurement of temperature rise on the friction interface was taken by a platinum resistance sensor, which was placed underneath the friction plate. The control system for the PE-SSA was designed as an open-loop system and implemented with DSPACE and MATLAB/SIMULINK. The whole system was further put in a chamber where the temperature inside the chamber was strictly controlled. The chamber was put on a vibration isolated test bed in order to reduce disturbances to the PE-SSA system (Fig. 8).

In the experiment, the temperature inside the chamber was controlled with a heater in the chamber. The voltage applied to the PEA was a repeating sawtooth wave with the amplitude of 30 V and the frequency of 5 Hz. When temperature varies, the displacements of the PE-SSA were measured at different temperatures.

Figure 9 shows the measured displacement (markers) of the actuator and the predicted displacement (solid lines) using Model I. The maximum prediction error of approximate 7% can be observed in Fig. 9 at 35.7 and 41.5 °C. Figure 10 shows the measured (markers) displacement of the actuator and the predicted (solid line) displacement using Model II. The maximum prediction of Model II is 8% at 35.7 °C only.

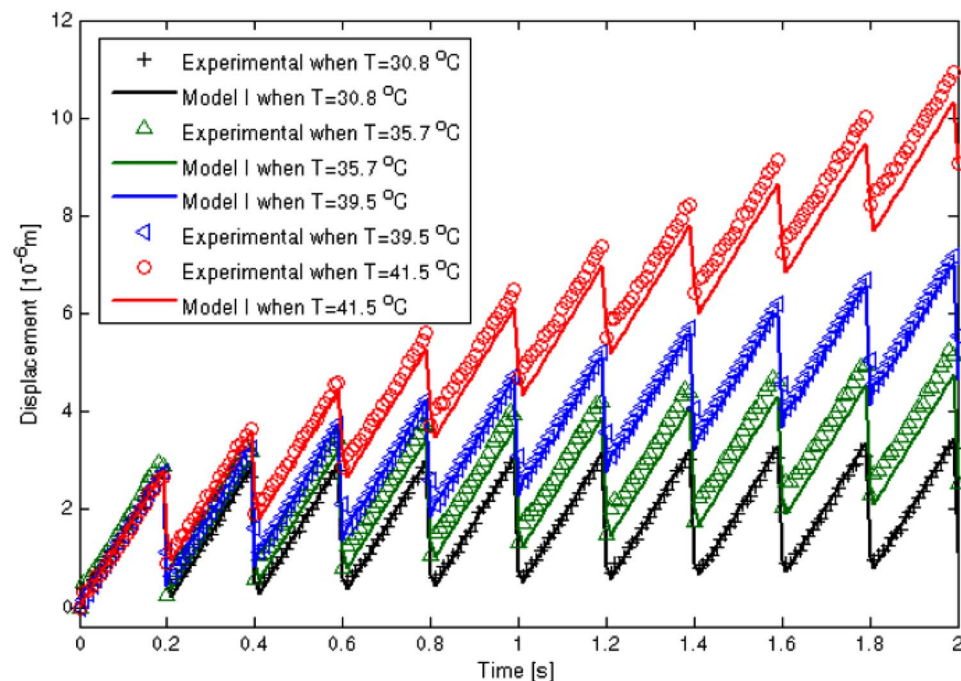


FIG. 9. (Color online) Measured and simulation results of Model I.

Therefore, the two models have nearly similar prediction accuracy. A more close examination can find that the average of maximum error with Model II is much smaller than that with Model I. Further, it is noted that Model I demands extremely high computational cost than Model II. In developing Model I, for every temperature point, determination of the three parameters took about 2 h. The total computational time for developing Model I took about 16–20 h. However, the total computational time for developing Model II took seconds. In fact, the computation for system identification for Model II is only relevant to a combined two linear equations. The following discussion is based on Model II.

From Fig. 10, it can be found that friction force decreases with the increase in temperature, which is in line

with Ref. 8 but not with Ref. 4. The reason for this is perhaps such that in our study and the study in Ref. 8, the work load on frictional surfaces is very small compared to that in the braking system studied in Ref. 4 and thus, temperature rise in our case as well as the case in Ref. 8 may lead to much easier deformation of asperities on the frictional surfaces (i.e., the increase in temperature may reduce the yield strength of the asperities). Further, because of such a relationship between friction force and temperature, the displacements of the actuator increase with the increase in temperature. This phenomenon can also be observed from Eq. (13) as well as Figs. 9 and 10 (respectively). In particular, during each slip motion period, the relative displacement between the stage and end effector increases due to the reduction in friction.

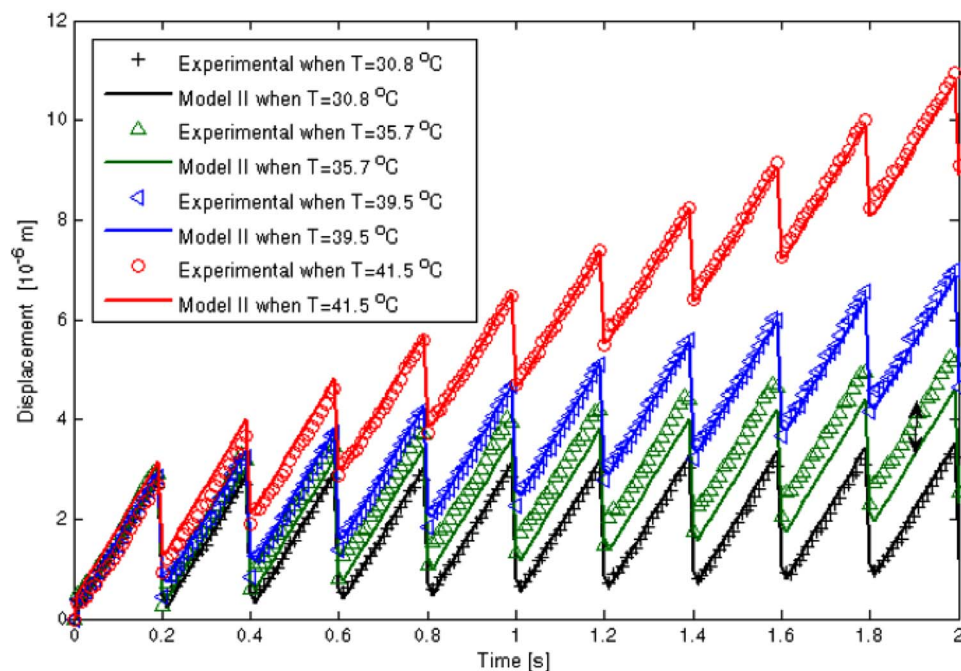


FIG. 10. (Color online) Experimental and simulation results of Model II (Temperature changes from 30.8 to 41.5 °C).

From Fig. 6, it is seen that the relationship between friction force and temperature appears to be nonlinear, and the nonlinear function seems to be well fit by two linear functions. In Ref. 8, however, friction seems to be quite linear with respect to temperature. This may be because the study in Ref. 8 was to observe friction force under the setting where two single asperities, from each of two atoms (respectively), contact one another; whereas in our situation, the distribution of asperities on the frictional surface is irregular and our study was to observe friction force under the setting where two groups of irregular asperities contact each other.

There is another interesting observation from this study. In our previous study in Ref. 6, we found that for the system of Fig. 1, if temperature changes only in the range of about 0.4 °C, the displacement of the actuator was not affected if the input voltage of the PEA is about 30 V. However, our current study clearly shows that the displacement of the actuator can be affected under the input voltage of 30 V for the temperature change being in the range of 10 °C.

V. CONCLUSION

We observed that in micromotion systems, such as PE-SSA, there can be a slight temperature rise, which has significant effect on friction force and thus on the performance of the systems.⁶ This finding has motivated us to model such thermal effects on friction force systematically. As such, two friction models were developed and presented in this paper, and both are based on the LuGre model. The experiment was conducted, and the experimental result and simulation results with the two models were compared.

The study can conclude: (1) both models can capture the characteristics of the friction-temperature relation and can show the same trend of exhibiting the friction behavior with respect to temperature, (2) Model II is better than Model I in terms of prediction accuracy and computational cost, (3) the friction force in the micromotion system decreases with the increase in temperature, (4) when the temperature change range is about 10 °C, the effect of temperature change on the displacement performance in the case of the PE-SSA is significant regardless of whether the input voltage to the PEA is high (30 V) or low (6 V), and (5) the procedure of developing Model II may be extended to other friction models (in particular, these other friction models will replace the LuGre model while the whole process will be kept the same), as the

same argument for the base model employed in this paper (i.e., the LuGre model) to incorporate thermal effects seems to be valid to other friction models as well.

ACKNOWLEDGMENTS

This paper presents the work partially completed when the first author was on a M. Sc. program at the East China University of Science and Technology and the work partially performed at the University of Saskatchewan when he worked as a visiting researcher. The financial support from the NSERC grant is acknowledged. We also want to thank Mr. Dong Kang and Mr. Qingshu Zhang for their pioneer work and assistance in building the test bed.

- ¹Y. Zhang, W. J. Zhang, J. Hesselbach, and H. Kerle, *Rev. Sci. Instrum.* **77**, 035112 (2006).
- ²D. Kang, Thesis of Master of Science, University of Saskatchewan (2007).
- ³T. H. C. Childs, *Wear* **260**, 310 (2006).
- ⁴A. L. Cristol-Bulthé, Y. Desplanques, and G. Degallaix, *Wear* **263**, 1230 (2007).
- ⁵T. A. Harris and M. N. Kotzalas, (Taylor & Francis, Boca Raton, FL, 2007).
- ⁶J. W. Li, G. S. Yang, W. J. Zhang, S. D. Tu, and X. B. Chen, *Rev. Sci. Instrum.* **79**, 046108 (2008).
- ⁷J. W. Li, W. J. Zhang, G. S. Yang, S. D. Tu, and X. B. Chen, *Int. J. Adv. Manuf. Technol.* (2008).
- ⁸Y. Sang, M. Dubé, and M. Grant, *Phys. Rev. Lett.* **87**, 174301 (2001).
- ⁹P. Dupont, B. Armstrong, and V. Hayward, *Proc. Amer. Control Conf.*, Chicago IL, 1072–1077 (2000).
- ¹⁰C. Canudas de Wit, H. Olsson, K. J. Åström, and P. Lischinsky, *IEEE Trans. Autom. Control* **40**, 419 (1995).
- ¹¹P. Dupont, V. Hayward, B. Armstrong, and F. Altpeter, *IEEE Trans. Autom. Control* **47**, 787 (2002).
- ¹²V. Lampaert, J. Swevers, and F. Al-Bender, *IEEE Trans. Autom. Control* **47**, 683 (2002).
- ¹³J. Swevers, F. Al-Bender, C. G. Ganseman, and T. Prajogo, *IEEE Trans. Autom. Control* **45**, 675 (2000).
- ¹⁴V. Lampaert, F. Al-Bender, and J. Swevers, *Proceedings of the IEEE International Conference on Physics and Control*, St. Petersburg, Russia, Aug. 2003, pp. 1170–1177 (unpublished).
- ¹⁵F. Al-Bender, V. Lampaert, and J. Swevers, *IEEE Trans. Autom. Control* **50**, 1883 (2005).
- ¹⁶H. J. M. T. A. Adriaens, W. L. de Koning, and R. Banning, *IEEE/ASME Trans. Mechatron.* **5**, 331 (2000).
- ¹⁷Q. S. Zhang, Thesis of Master of Science, University of Saskatchewan (2008).
- ¹⁸E. Baker, *IEEE Trans. Parts Hybrids Packag.* **8**, 4 (1972).
- ¹⁹A. B. Lebedev, Y. A. Burenkov, A. E. Romanov, V. I. Kopylov, V. P. Filonenko, and V. G. Gryaznov, *Mater. Sci. Eng., A* **203**, 165 (1995).
- ²⁰T. H. Fang, C. I. Weng, and J. G. Chang, *Mater. Sci. Eng., A* **357**, 7 (2003).